Optimization of the spatial light modulation with twisted nematic liquid crystals by a genetic algorithm

Joonku Hahn, Hwi Kim, and Byoungho Lee*
School of Electrical Engineering, Seoul National University, Gwanak-Gu Sinlim-Dong, Seoul 151-744, South Korea
*Corresponding author: byoungho@snu.ac.kr

Received 12 October 2007; revised 22 January 2008; accepted 22 January 2008;
posted 24 January 2008 (Doc. ID 88506); published 17 March 2008

An optimization technique determining the configuration of optical components in a spatial light modulator is proposed. We study a spatial light modulator composed of a twisted nematic liquid crystal, a polarization state generator, and a polarization state detector. To obtain the desired phase and amplitude modulations, four parameters of the polarization state generator and detector should be optimized. A genetic algorithm is applied in searching the configurations suitable to a given twisted nematic liquid crystal. By embodying the proposed technique, the evolution of the designed cost functions is proved. © 2008 Optical Society of America

OCIS codes: 050.1970, 090.2890, 160.3710, 230.6120.

1. Introduction

Spatial light modulators (SLMs) are used in a wide range of applications, including telecommunication, displays, optical storage, and optical information processing, and they are researched intensively. In digital holography, resolution and pixel pitch of the SLM affect the quality and size of diffraction images. Commercial twisted nematic liquid crystals (TNLCs) for projection display have a lot of pixels, with the size as small as several tens of micrometers; therefore SLMs based on TNLC prevail for phase or amplitude modulations by the development of the projection display industry.

The propagation of the light in TNLC is perfectly described with the extended Jones matrix [1,2]. However, practically the optical structure of TNLC is simply modeled to obtain the characteristic parameters in experimental results. The most simplified model regards TNLC as a polarization rotator with cascaded wave plates [3]. After that, some advanced models are proposed taking account of edge effects of TNLC so that the molecules near both alignment layers do not tilt independent of an electric field [4–6]. To estimate the modulation through a given TNLC by simulation, the characteristic parameters of the model of TNLC should be determined through experiments. Even in the most simplified model, there are ambiguities in the measurement of only three characteristic parameters [7], and troublesome methods are required to exclude these ambiguities.

Phase and amplitude modulations through TNLC are intuitively understood by the concept of polarization eigenstates based on the most simplified model [8]. With the help of these polarization eigenstates, modulation behaviors of some SLMs are predicted and compared with experimental results [9,10]. For convenience, the input and output polarization states are able to be defined as a polarization state generator (PSG) and a polarization state detector (PSD) [11]. Recently, to obtain phase-only modulations with TNLC, the techniques of analyzing the polarization states on the Poincaré sphere are actively studied [12,13]. However, since the thickness of the TNLC decreases on account of smaller pixels and faster response, the edge effects of TNLC become more significant, and the most simplified model that neglects edge effects is insufficient to predict the modulation behavior.

0003-6935/08/190D87-09$15.00/0

The thinner TNLC is, the more incorrect the simplified model is. In addition, a complicated model requires more characteristic parameters, and in the measurement of the characteristic parameters it is troublesome to exclude the ambiguities. Therefore we approach the optimization of an SLM, not by modeling TNLC, measuring characteristic parameters, and predicting the modulation behavior with a computation, but by changing the PSG and PSD configurations and measuring the modulation behavior. In this approach we measure directly the modulation behavior of an SLM depending on the applied voltage; therefore the optimization procedures are simplified and free of the errors resulting from modeling and measuring processes.

In an optimization problem of several parameters, a genetic algorithm effectively finds a proper solution [14]. In a digital holographic beam-shaping system, optimization of encoding index and compensation of an aberration is proposed using a genetic feedback loop [15]. In this paper, we embedded the genetic algorithm in the SLM system, simultaneously measuring the phase and amplitude modulation according to the applied voltage when controlling the rotation angles of the optics with motorized stages. Many techniques measuring the phase modulation of an SLM have been studied [16–18]. In this paper, a wavefront interferometer using double slits is applied.

This paper is organized as follows. In Section 2, the configuration of the SLM using TNLC is described on the Poincaré sphere. An ideal TNLC is expressed as polarization eigenstates, and the edge effects are discussed. The configuration parameters of the PSG and PSD appended to the TNLC are defined. In Section 3, the proposed genetic optimization technique is described. The chromosome and procedure of the genetic algorithm are detailed, and the structure of the program is described. In Section 4, the system embodying the proposed algorithm is described, and the experimental results are discussed. For the designed cost function, the optimization of the SLM is presented. In Section 5, concluding remarks and perspectives on the devised system are provided.

2. Spatial Light Modulation Using a Twisted Nematic Liquid Crystal Device

In this section, optical components in a general configuration of the SLM using TNLC are represented on the Poincaré sphere, and the configuration parameters for optimizing the SLM are defined. In the ideal TNLC, the eigenstates are elliptic polarization states, and the eigenvalues are phase delays of the light going through TNLC. To obtain a large phase modulation, the eigenstate with a large change in its eigenvalue according to the applied voltage has to be chosen. The edge effects are comprehensible to shift the eigenstates around director axes on the Poincaré sphere, and the shifted eigenstates do not have the same inclination angle of the polarization ellipse as the applied voltage of TNLC changes. Therefore, these variations in the inclination angles require a proper PSG and PSD appended to TNLC to choose the eigenstate with the more desirable phase modulation in the change of the applied voltage.

The general configuration of the SLM using TNLC is shown in Fig. 1, where a polarizer and a wave plate before TNLC construct a PSG, and a wave plate and a polarizer after TNLC construct a PSD. The $\hat{x}$ axis is parallel to the director axis on the input plane of TNLC, and the $\hat{z}$ axis is the direction of light propagation. The angles of polarizers, θ_{P1} and θ_{P2}, are defined as the rotations of polarization axes, and the angles of wave plates, θ_{W1} and θ_{W2}, are defined as the rotations of fast axes from the $\hat{x}$ axis.

An elliptic polarization state can be expressed by the azimuth angle of the oscillation direction ψ and a relative phase δ, and this is related to Jones vector representation by

$$(\delta, \psi) \equiv \begin{pmatrix} \cos\ \psi \\ e^{i\delta}\ \sin\ \psi \end{pmatrix}. \tag{1}$$

Figure 2 shows the elliptic polarization state in xy plane and its position on the Poincaré sphere, where the inclination angle of the polarization ellipse ϕ and the ellipticity angle ε is defined by

$$\sin\ 2\varepsilon \equiv \sin\ 2\psi\ \sin\ \delta, \tag{2a}$$

$$\tan\ 2\phi \equiv \tan\ 2\psi\ \cos\ \delta. \tag{2b}$$

In this paper we represent an ideal TNLC with the edge effects on the Poincaré sphere, since there are not many studies about the shifts of eigenstates owing to the edge effects. Figure 3 shows twist angles and birefringences as a function of TNLC depth in ideal case models. In Figs. 3(a) and 3(b), the simplest model is shown that was proposed by Lu and Saleh [3], and in Figs. 3(c) and 3(d), the more advanced

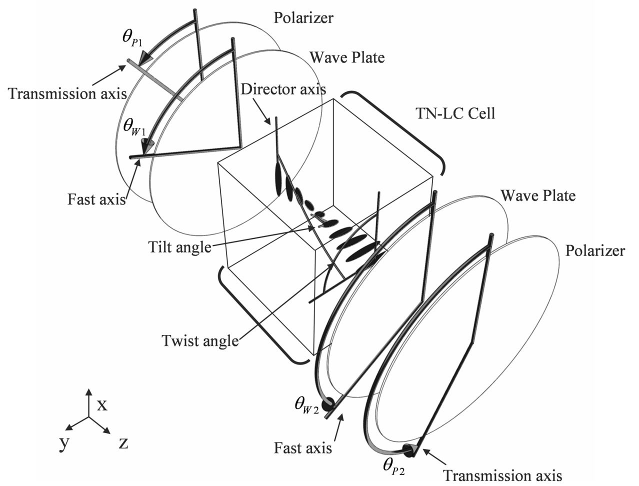

Fig. 1. Schematic of the SLM composed of TNLC, a polarization state generator, and a polarization state detector: θ_{P1} and θ_{P2} are rotation angles of input and output polarizers; θ_{W1} and θ_{W2} are rotation angles of input and output wave plates.

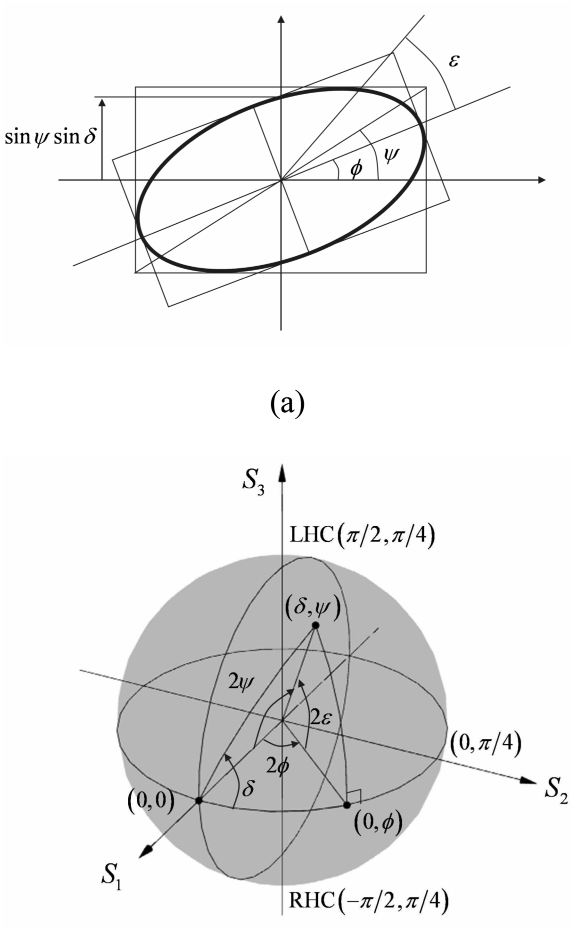

(a)

(b)

Fig. 2. Elliptic polarization state (a) in the *xy* plane and (b) its position on the Poincaré sphere.

model with the edge effect is shown that was proposed by Coy *et al.* [4]. In Figs. 3(c) and 3(d), except for the edge of the TNLC with the thickness t, on both sides the twist angle increases linearly according to the TNLC depth, and the birefringence is uniform regardless of the TNLC depth. These bulk properties of the TNLC are the same as the Lu and Saleh model [3]. Therefore, the model proposed by Coy *et al.* [4] is equivalent to the summation of the bulk TNLC model and the wave plates on both edges.

The Jones matrix M_{TNLC} for TNLC with edge effect can be represented as

$$\begin{aligned} M_{\mathrm{TNLC}} &= R(-\alpha)W(2\pi t\Delta n/\lambda)R(\alpha)M_{\mathrm{bulk\,TNLC}}W(2\pi t\Delta n/\lambda) \\ &= \exp(-i\beta)R(-\alpha)W(2\pi t\Delta n/\lambda)M(\alpha,\beta)W(2\pi t\Delta n/\lambda), \end{aligned} \tag{3}$$

where $M_{\mathrm{bulk\,TNLC}}$ for the bulk TNLC is given by

$$M_{\mathrm{bulk\,TNLC}} = \exp(-i\beta)R(-\alpha)M(\alpha,\beta). \tag{4}$$

Here the rotation matrix $R(\theta)$ is defined by

$$R(\theta) = \begin{bmatrix} \cos\,\theta & \sin\,\theta \\ -\sin\,\theta & \cos\,\theta \end{bmatrix}, \tag{5}$$

and the phase shift matrix $W(\varphi)$ is defined by

$$W(\varphi) = \begin{bmatrix} 1 & 0 \\ 0 & \exp(i\varphi) \end{bmatrix}. \tag{6}$$

The matrix $M(\alpha,\beta)$ is given by

$$M(\alpha,\beta) = \begin{bmatrix} \cos\,\gamma - i\beta\,\sin\,\gamma/\gamma & \alpha\,\sin\,\gamma/\gamma \\ -\alpha\,\sin\,\gamma/\gamma & \cos\,\gamma + i\beta\,\sin\,\gamma/\gamma \end{bmatrix}. \tag{7}$$

Here β is the birefringence, α is the twist angle, and $\gamma^2 = \alpha^2 + \beta^2$. The birefringence β is given by

$$\beta = \pi(d - 2t)\Delta n_{\mathrm{eff}}/\lambda, \tag{8}$$

where $(d - 2t)$ is the thickness of a bulk TNLC, λ is the incident wavelength, and Δn_{eff} is the difference between the ordinary and the effective extraordinary indices of refraction perpendicular to the propagation.

Davis *et al.* derived the polarization eigenstates of the bulk TNLC model in Ref. [8] for the theoretical approach to phase modulation. The rotated eigenstates for the matrix $M(\alpha,\beta)$ are given by

$$E_\lambda(+) = \begin{bmatrix} \alpha/(2\gamma^2 + 2\beta\gamma)^{1/2} \\ i(\beta + \gamma)/(2\gamma^2 + 2\beta\gamma)^{1/2} \end{bmatrix}, \tag{9a}$$

$$E_\lambda(-) = \begin{bmatrix} (\beta + \gamma)/(2\gamma^2 + 2\beta\gamma)^{1/2} \\ -i\alpha/(2\gamma^2 + 2\beta\gamma)^{1/2} \end{bmatrix}. \tag{9b}$$

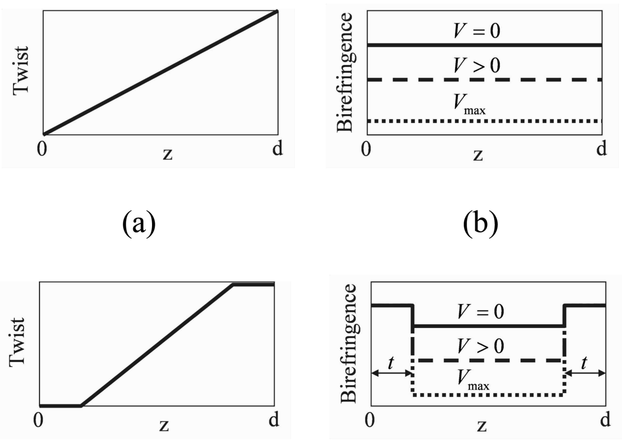

(a) (b)

(c) (d)

Fig. 3. Twist angles and birefringences as a function of TNLC depth: (a), (b) Lu and Saleh model; (c), (d) Coy *et al.* model.

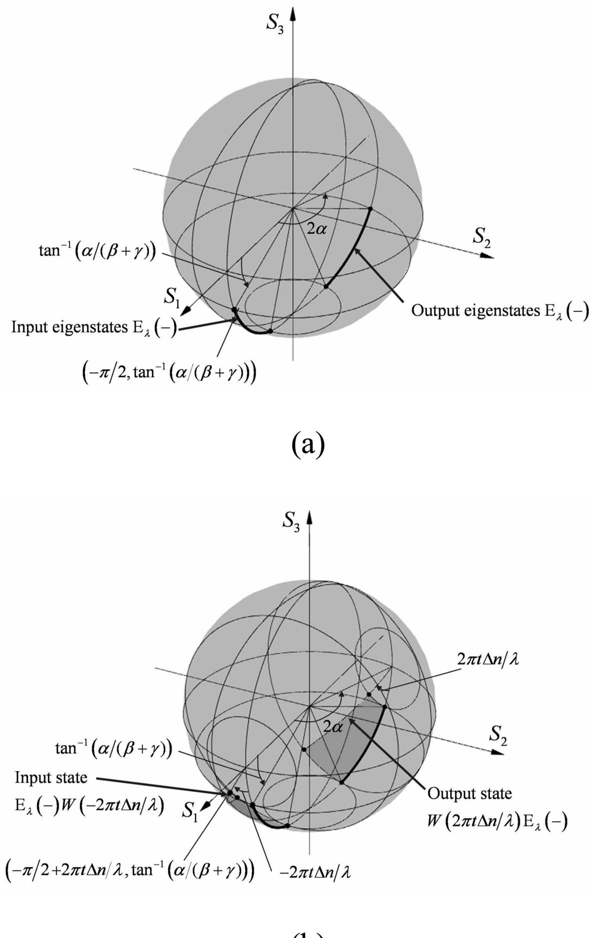

Fig. 4. Input and output negative eigenstates $E_\lambda(-)$ on the Poincaré sphere, and their traces according to the applied voltage (a) without and (b) with the edge effect.

Here their eigenvalues are given by

$$\lambda(\pm) = \exp(-i\beta)\ \exp(\pm i\gamma). \tag{10}$$

Therefore, the negative eigenstate $E_\lambda(-)$ has larger phase delay than the positive eigenstate $E_\lambda(+)$. In most cases, the SLM is optimized to maximize the phase modulation up to 2π, and the negative eigenstate $E_\lambda(-)$ is important for designing the PSG and PSD configurations.

Figure 4(a) shows the input and output negative eigenstates $E_\lambda(-)$ on the Poincaré sphere and their traces according to the applied voltage. In Eq. (9b), the relative phase and azimuth angle of the input negative eigenstates are given by

$$\delta = -\pi/2, \tag{11a}$$

$$\psi = \tan^{-1}[\alpha/(\beta+\gamma)]. \tag{11b}$$

The output negative eigenstates are rotated by 2α around the S_3 axis on the Poincaré sphere. In Eq. (8) the birefringence β is a function of the applied voltage V defined by

$$\Delta n_{\text{eff}} = \sqrt{\frac{n_e^2 n_o^2}{n_e^2\sin^2\theta_{\text{tilt}}(V) + n_o^2\cos^2\theta_{\text{tilt}}(V)}} - n_o. \tag{12}$$

Here, $\theta_{\text{tilt}}(V)$ is the tilt angle of liquid crystal molecules in the bulk TNLC, and n_o and n_e represent the ordinary and extraordinary indices in the molecule, respectively. This tilt angle increases monotonously according to the applied voltage, which is represented as

$$\theta_{\text{tilt}}(V_i) \geq \theta_{\text{tilt}}(V_j) \quad \text{if } V_i > V_j. \tag{13}$$

Therefore, the birefringence decreases as the applied voltage increases, and negative eigenstates trace to the right handed circle (RHC) point ($\delta = -\pi/2$, $\psi = \pi/4$) with the same inclination angles of the polarization ellipse ϕ. Figure 4(b) shows the shifts of input and output negative eigenstates owing to the edge effect. The input negative eigenstate $E_\lambda(-)$ shifts by the negative phase $-2\pi t\Delta n/\lambda$, and the resultant state is at $(-\pi/2 + 2\pi t\Delta n/\lambda, \tan^{-1}[\alpha/(\beta+\gamma)])$. On the contrary, the output negative eigenstate $E_\lambda(-)$ shifts by the positive phase $2\pi t\Delta n/\lambda$. Therefore, the edge effects result in the rotation of input and output negative eigenstates around the central points $(0, 0)$ and $(0, \alpha)$, respectively. That is, these elliptic polarization states on the shifted traces do not have the same inclination angle of the polarization ellipse. Even though we discussed the ideal TNLC proposed by Coy *et al.* [4], it is obvious for most nonreflective TNLC models that there are elliptic polarization eigenstates whose inclination angles vary according to the applied voltage.

In the hypothetical case that the negative eigenstates are placed near the points $(0, 0)$ and $(0, \alpha)$ regardless of the applied voltage on the Poincaré sphere, the PSG and PSD can be simplified as linear polarizers to choose the demanded negative eigenstates. However, in a practical TNLC the eigenstates become close to the circular polarization state as the applied voltage increases, and the edge effects shift these eigenstates changing the inclination angle of the polarization ellipse. Therefore, proper configurations of PSG and PSD are necessary to attain the desirable phase modulation using TNLC.

Figure 5 shows PSG and PSD constructed with quarter wave plates on the Poincaré sphere. In Fig. 5(a), the bold curve means the conversion from $(0, \theta_{\text{P1}})$ to (δ, ψ) by the PSG. The input beam of an SLM should be circularly polarized for the uniform transmittance through the PSG since the first component of the PSG is a linear polarizer. Any elliptic polarization state can be generated with two variable angles θ_{P1} and θ_{W1} satisfying

$$\sin\ 2(\theta_{\text{W1}} - \theta_{\text{P1}}) = \sin\ 2\psi\ \sin\ \delta, \tag{14a}$$

$$\tan\ 2\theta_{\text{W1}} = \tan\ 2\psi\ \cos\ \delta. \tag{14b}$$

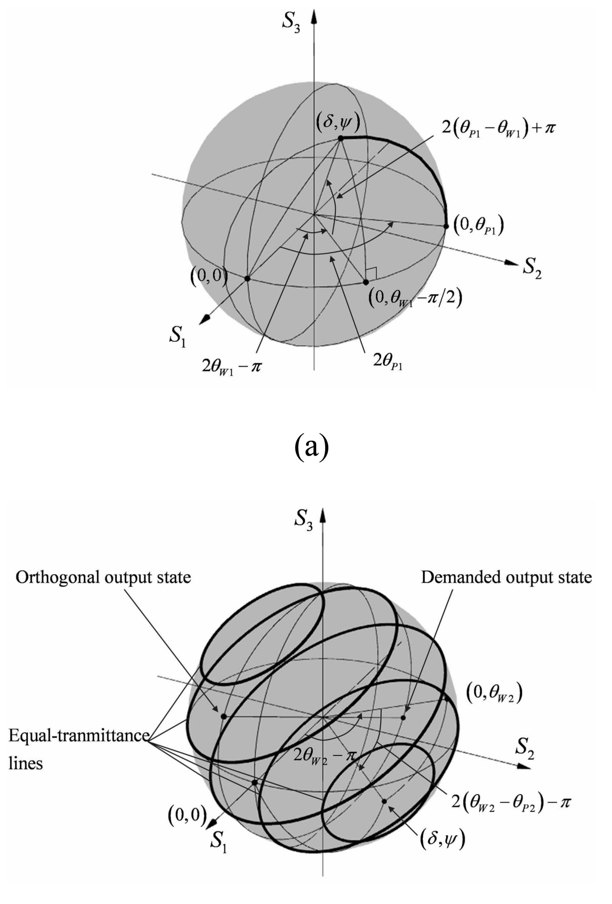

(a)

(b)

Fig. 5. Elliptic polarization states of (a) PSG and (b) PSD on the Poincaré sphere.

Similarly, the relative phase and azimuth angle of the elliptic polarization state in the PSD satisfy

$$\sin\ 2(\theta_{\mathrm{P2}}-\theta_{\mathrm{W2}})=\sin\ 2\psi\ \sin\ \delta, \tag{15a}$$

$$\tan\ 2\theta_{\mathrm{W2}}=\tan\ 2\psi\ \cos\ \delta. \tag{15b}$$

In Fig. 5(b), the bold curves mean the polarization states with equal transmittances chosen by this PSD.

The PSG and PSD have the fixed points on the Poincaré sphere even though the negative eigenstate of TNLC moves according to the applied voltage. So it is impossible to select only the negative eigenstate over the range of the applied voltage. Since the positive eigenstate is orthogonal to the negative eigenstate in spite of the phase shift owing to the edge effect, the contributions of two eigenstates defined by PSG and PSD are trigonometrical functions. Therefore, the phase modulations resulting from the combination of two eigenstates are generated and detected over the range of the applied voltage, and the fittest configuration of PSG and PSD is searched for the desired SLM.

3. Genetic Optimization Algorithm

In this section, the proposed genetic optimization technique is described. The chromosome and procedure of the genetic algorithm are detailed, and the structure of the program is described.

Figure 6 shows the schematic of the system optimizing the SLM with a genetic algorithm. First, the collimated beam is expanded and circularly polarized through the quarter wave plate. Next, the circularly polarized beam enters a PSG and is converted to a designed elliptic polarization state. Next, this beam passes the mask with double slits and an aperture before the TNLC. The double slits function as a wave-front interferometer to measure phase modulations, and a larger aperture exists to measure amplitude modulations. Next, the beam enters the TNLC for a light modulation. As previously discussed, the elliptic polarization state generated by the PSG travels on the Poincaré sphere according to applied voltage. Next, the modulated beam passes through the PSD and is converted to a linear polarization state. Last, beams through the double slits and the aperture on the mask are collected by the lenses at the front of a charge-coupled device (CCD) and an optical power meter (OPM), respectively. The loop of genetic algorithm is constructed between measurement and modulation through a computer. The cost value of a genetic algorithm is evaluated from data of the CCD and the OPM under a full range of applied voltage. The rotation stages are controlled and the encoding index of the TNLC is changed by the computer.

In general, a genetic algorithm has two operations to search local optima. The crossover operation is effective in convex optimization problem, since it is mathematically analogous to the linear combination of two chromosomes in a floating point coding scheme. The mutation operation is effective in a general optimization problem since it makes the small variations of the present solution and searches the optimum solution randomly. Therefore the mutation operation is more essential in the genetic algorithm, and we employ only this operation in our application.

In this genetic algorithm, a chromosome is composed of four configuration parameters of the SLM.

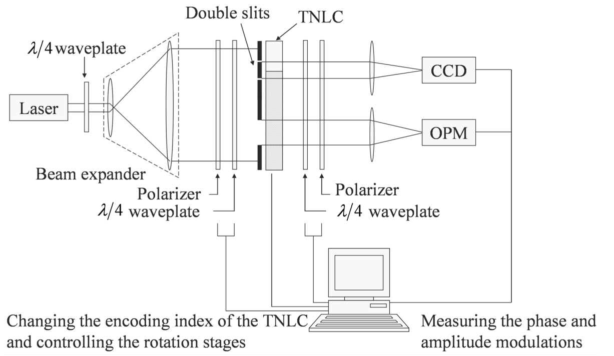

Fig. 6. Schematic of the system optimizing the SLM with genetic algorithm.

The angles of polarizer θ_{P1} and the angles of wave plate θ_{W1} define the PSG, and the angles of polarizer θ_{P2} and the angles of wave plate θ_{W2} define the PSD. These angles have the freedom from 0 to π. Hence, the cost function F is parameterized by the chromosome, and the optimization problem is defined as

$$\max\ F[\theta_{P1}, \theta_{W1}, \theta_{P2}, \theta_{W2}] \quad \text{for } 0 \le \theta_{P1}, \theta_{W1}, \theta_{P2}, \text{ and } \quad \theta_{W2} \le \pi. \tag{16}$$

Here the formula of F is completely described in the next section.

Figure 7 shows the flow chart of the genetic algorithm implemented with Labview and Matlab. In this flow, Labview controls the motorized stages changing the angles of optics and measures the amplitude and phase modulations, and Matlab manages the genetic algorithm and computes the cost function. These two programs are able to be connected with the Math script in Labview, and Matlab is inserted in Labview as the object. Even though the main stream of the genetic algorithm is programmed with Matlab, the flow is started and ended by Labview. The system parameters and measured data are transferred to each other as variables. Therefore, we programmed that Matlab memorizes the whole data set for generations and that Labview calls demanded current variables.

In Fig. 7, the flow follows a general genetic algorithm with the mutation operator. First, the initial population P_0 with a population size m is selected. In this paper, we set the population size to be five, and this population is composed of chromosome x_i having four elements in accordance with the rotation angles. Next, the cost values $F(P_{k=0})$ of chromosomes in the initial population are calculated, and the fittest chromosome having the largest cost value, i.e., the elite $\bar{x}$, is determined. Next, the mutation operation is applied to the initial population $P_{k=0}$, and then the modified population $\bar{P}'_{k=0}$ is obtained. In the mutation operator for floating point coding, the mutation probability and the system parameter determining the degree of nonuniformity are tuned to about 0.5 and 1.5. Next, the cost values $F(\bar{P}'_{k=0})$ of chromosomes in the mutated population are calculated, and the fittest chromosome $\hat{x}$ is determined. Next, the new fittest chromosome $\tilde{x}$ is selected from $\bar{x}$ and $\hat{x}$. Last, the population is reorganized, and the new fittest chromosome copies itself by clone size h times. These sequences are repeated until the $k_{\max}$th generation.

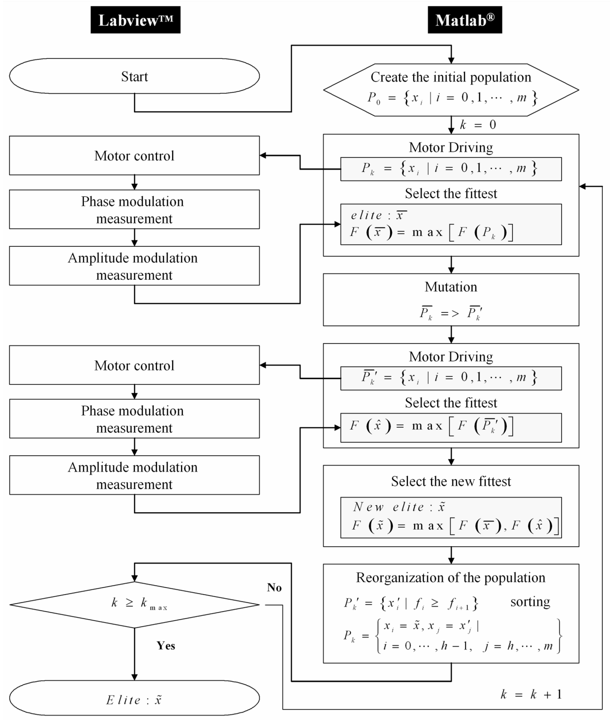

Fig. 7. Flow chart of the genetic algorithm implemented with Labview and Matlab.

The main virtual instrument (VI) has three sub-VIs, and each sub-VI calls the functions in data acquisition (DAQ) and image acquisition (IMAQ) libraries. The first sub-VI measures the amplitude modulations of an SLM at 17 encoding indices, the values of which are spaced at an interval of 2^4. The number of encoding indices is determined to obtain a curve of amplitude modulations efficiently and to avoid the failure to notice singular points in the curve. This sub-VI is composed of IMAQ functions to encode the SLM and a general purpose interface bus (GPIB) function to communicate with the OPM. The second sub-VI measures the phase modulations of an SLM at 9 encoding indices, the values of which are spaced at an interval of 2^5. The transmission is determined by polarizations, and the amplitude modulation could decrease to zero. On the other hand, the phase modulation is determined by the refractive index of liquid crystal molecules. Since the liquid crystal molecule rotates to the position where the elastic distortion force is equivalent to the electric force, generally there is no abrupt change in the liquid crystal molecule according to the applied voltage. Therefore, the phase modulation varies slowly according to an encoding index, and, to obtain a curve of phase modulations, a relatively small number of measurements is required. This sub-VIs are composed of IMAQ functions to encode the SLM and communicate with a CCD through an IMAQ board. To raise the communication speed with the CCD, the size of the region of interest is reduced to 200 × 5 pixels. The third sub-VI drives the motorized rotation stages with a full-step resolution. The DAQ board is used to control the step motor driver. In the event, the whole process of a single generation takes about 25 seconds.

4. Experimental Embodiment of the Optimization System

In this section, the system embodying the proposed algorithm is described and the experimental results are discussed. The technique for measuring the phase modulation is detailed, and a devised economic motorized stage is explained. The cost function is formulated for maximizing the phase modulation, and the evolution of the SLM is discussed.

In this paper, the wave-front interferometer is used for measuring the phase modulation. The interferometer splits the incident wave front with double slits and observes the interference resulting from different path lengths in the same optical arm. The beam through one slit functions as a reference and is modulated by the SLM with a fixed encoding index. The beam through the other slit functions as a signal and is modulated by the SLM with designed encoding index. In this interferogram, the fringe moves according to the phase shift of the signal beam. When the incident beam with a wavelength λ passes through the double slits with a gap Δ and is collected by a lens with a focal length f, an interference term of this interferogram on the CCD with pixel pitch p_{CCD} can be represented as

$$I_{\mathrm{int}}(p_j) = I_{\mathrm{int},0}\cos(2\pi p_j/\Lambda + M_{\mathrm{Phase}}). \tag{17}$$

Here, Λ is the period of a fringe, and p_j is the position on the CCD. The phase modulation M_{Phase} of the signal beam appears in the argument of a cosine function. In the paraxial approximation, Λ is given by

$$\Lambda = f\lambda/\Delta, \tag{18}$$

and p_j is defined by

$$p_j = p_{\mathrm{CCD}} \times (j-1). \tag{19}$$

The phase shift can be simply calculated from the amount of a fringe shift over the period. However, we calculate the phase shift by a discrete Fourier transform and increase the accuracy. The discrete Fourier transform of $I_{\mathrm{int}}(p_j)$ is defined by

$$X(k) = \sum_{j=1}^{N} I_{\mathrm{int},0}\cos(2\pi p_j/\Lambda + M_{\mathrm{Phase}})\,\omega_N^{(j-1)(k-1)}, \tag{20}$$

where N is the side length of the region of interest on the CCD over the pixel pitch, and ω_N is an Nth root of unity given by

$$\omega_N = \exp(-2\pi i/N). \tag{21}$$

The phase modulation M_{Phase} is calculated from

$$M_{\mathrm{Phase}} = \mathrm{unwrap}\{\mathrm{angle}[X(p_{\mathrm{CCD}}N/\Lambda + 1)]\}. \tag{22}$$

In this interferometer, the gap Δ of the double slits is designed to satisfy

$$\Delta = 4f\lambda/p_{\mathrm{CCD}}N. \tag{23}$$

The calculation using a discrete Fourier transform filters a signal in the frequency domain and averages the phase modulation by 4 times.

Figure 8 shows the experimental setup. In the system embodying the proposed algorithm, the optical parts are realized with the second harmonic Nd:YAG laser (Coherent Verdi V-5), the CCD (KODAK MegaPlus ES1.0/MV) with 9 μm pixel pitch, and the OPM (Newport 1835-C). The mechanical parts are actualized with motorized rotation stages and motor drivers. This motorized stage is driven by a two-phase step motor with a 1/5 inch pitch timing belt. The teeth of a timing pulley in an optical mount are twice those in a step motor, and two revolutions of the motor shaft are equal to one revolution of the optics.

In this paper, the cost function is designed to attain the maximum phase modulation of the SLM. In the genetic algorithm, chromosomes evolve to let the cost value down, and the cost function is formulated as

$$F(x_i) = \min(M_{\mathrm{Phase},i}) - \max(M_{\mathrm{Phase},i}). \tag{24}$$

Practically we have to exclude chromosomes having too low amplitude transmission $M_{\mathrm{Amp}}(16j-1)$ with $(16j-1)$th encoding index and set two exclusion conditions given by

$$\sum_{j=0}^{16}[M_{\mathrm{Amp}}(16j-1)]^2 \geq 10^{-5}\,(\mathrm{watt}), \tag{25a}$$

$$\frac{4\sum_{j=0}^{16}[M_{\mathrm{Amp}}(16j-1)]^2}{\sqrt{\sum_{j=0}^{16}\{[M_{\mathrm{Amp}}(16j-1)]^2 - \overline{M_{\mathrm{Amp}}{}^2}\}^2}} > 20. \tag{25b}$$

Here, $\overline{M_{\mathrm{Amp}}{}^2}$ is the average of transmittances defined by

$$\overline{M_{\mathrm{Amp}}{}^2} = \sum_{j=0}^{16}[M_{\mathrm{Amp}}(16j-1)]^2/17. \tag{26}$$

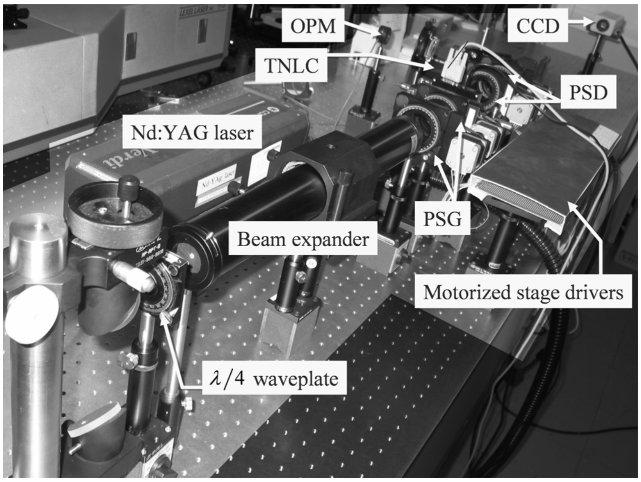

Fig. 8. Picture of the experimental setup.

By Eq. (25b), chromosomes with singular points in the amplitude transmission curve cannot survive.

We use TNLC made by SONY whose model number is LCX016AL-6. In this TNLC the contrast and brightness are set at 198 and 102, respectively, with the program Holoeye LC2002. Figure 9 shows characteristics of SLM during evolution and at stagnated state. Figures 9(a) and 9(b) show the evolution of phase modulation and amplitude transmission curves, respectively, for 100 generations. At stagnated state, the phase modulation and amplitude modulation are shown in Figs. 9(c) and 9(d), and the optimized configuration parameters of the SLM are listed in Table 1. In Fig. 9(a) the values of the phase modulation for generations are set to be zero at zeroth encoding index and the phase modulation increases monotonically. Therefore the phase modulations at the 255th encoding index are the maximum values for generations, and it is noticeable for the range of phase modulation to grow during the evolution. At stagnated state, consequently the range of phase modulations in the SLM reaches 6.05 (rad). As expected, no significant singular points are shown in the amplitude transmission curve at stagnated state, and the numerical value of the second exclusion condition Eq. (25b) is 41.7. With the proposed genetic system the SLM using TNLC is optimized to attain the desirable phase and amplitude modulations.

Figure 10 shows the diffraction images using the SLM. The digital hologram encoded on the SLM is generated by the iterative Fourier transform algorithm considering the functional relationship between phase and amplitude modulations [19]. In Fig. 10(a), the diffraction image is captured with the configurations at the first generation. The initial configuration uses classical linear polarized input and output states that are aligned parallel to each other. The SLM with the initial configuration has only 2.99 (rad) phase modulation, and the twin image appears definitely. In Fig. 10(b), the diffraction image is captured with the configurations at the

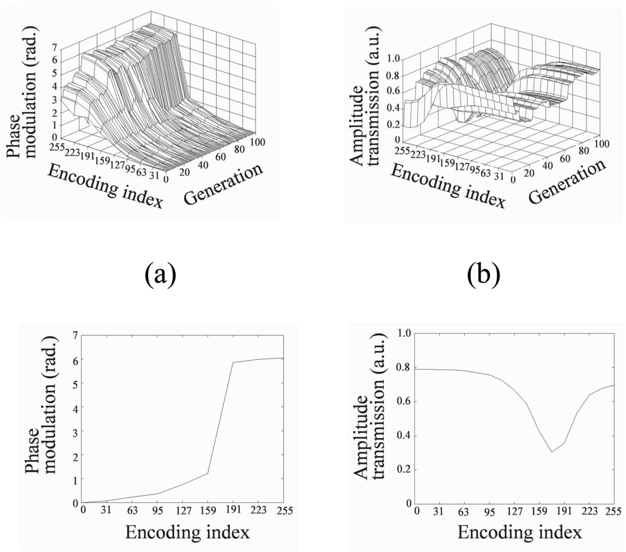

(a) (b)

(c) (d)

Fig. 9. (Color online) Characteristics of SLM during evolution and at stagnated state: (a) phase modulation and (b) amplitude transmission during evolution, and (c) phase modulation and (d) amplitude transmission at stagnated state.

Table 1. Optimized Configuration Parameters of the Spatial Light Modulator

Configuration Parameters	Rotation Angle (degree)
Input polarizer (θ_{P1})	14.4
Input wave plate (θ_{W1})	76.5
Output wave plate (θ_{W2})	30.6
Output polarizer (θ_{P2})	119.7

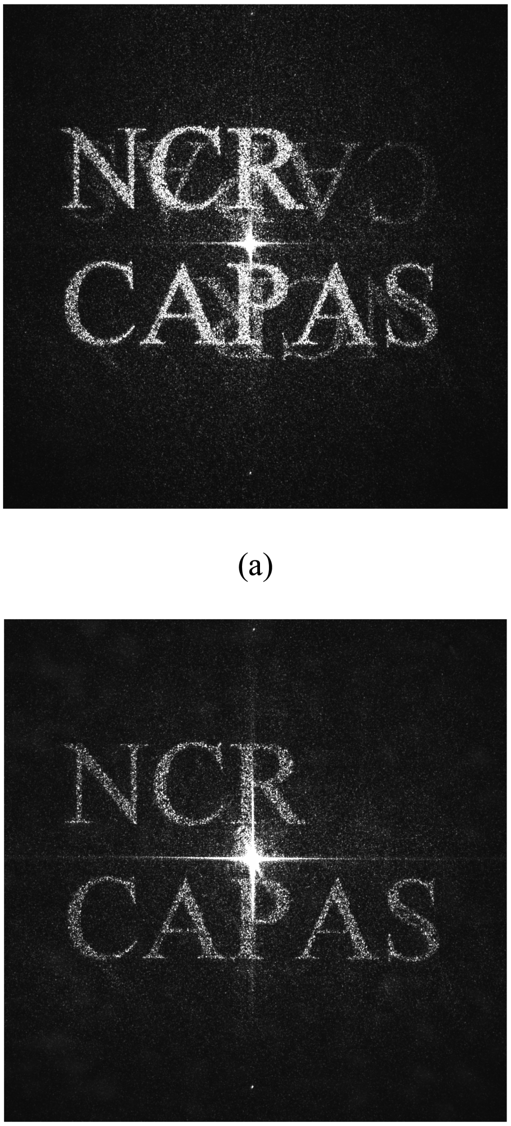

(a)

(b)

Fig. 10. Diffraction images using the SLM (a) at the first generation and (b) at the stagnated state after the genetic optimization.

stagnated state, and twin image is hard to distinguish. The existence of a twin image could be evaluated by the ratio of twin signal to original signal. The regions of twin and original signals are defined at the generation process by the iterative Fourier transform algorithm, and the ratio is calculated from the averaged intensities in each region. By this calculation we evaluate the ratios are 0.3271 and 0.0575 before and after the optimization, respectively, and it reflects that the troublesome twin image is reduced effectively after the genetic optimization.

5. Conclusion

In conclusion, it is shown that the genetic optimization technique is efficient to determine the configuration of an SLM. We represent the optical components of an SLM on the Poincaré sphere, and we show that eigenstates of TNLC do not have the same inclination angle according to the applied voltage since the edge effect of TNLC shifts eigenstates on the Poincaré sphere. Therefore we show that four parameters of the polarization state generator and detector are needed to define the characteristics of the SLM. In this genetic optimization system the phase and amplitude modulation are simultaneously measured according to applied voltages, and the phase shift is calculated using a discrete Fourier transform. It is expected that the proposed technique can be useful in optimizing the SLM using various kinds of commercial TNLCs to attain the desirable phase and amplitude modulation.

This work was supported by Samsung SDI, Ltd.

References

1. A. Lien, "A detailed derivation of extended Jones matrix representation for twisted nematic liquid crystal displays," Liq. Cryst. **22**, 171–175 (1997).
2. P. Yeh and C. Gu, *Optics of Liquid Crystal Display* (Wiley, 1999).
3. B. E. A. Saleh and K. Lu, "Theory and design of the liquid crystal TV as an optical spatial phase modulator," Opt. Eng. **29**, 240–246 (1990).
4. J. A. Coy, M. Zaldarriaga, D. F. Grosz, and O. E. Martínez, "Characterization of a liquid crystal television as a programmable spatial light modulator," Opt. Eng. **35**, 15–19 (1996).
5. A. Márquez, J. Campos, M. J. Yzuel, I. Moreno, J. A. Davis, C. Iemmi, A. Moreno, and A. Robert, "Characterization of edge effects in twisted nematic liquid crystal displays," Opt. Eng. **39**, 3301–3307 (2000).
6. Q. Wang and S. He, "A new effective model for the director distribution of a twisted nematic liquid crystal cell," J. Opt. A: Pure Appl. Opt. **7**, 438–444 (2005).
7. J. A. Davis, D. B. Allison, K. G. D'Nelly, M. L. Wilson, and I. Moreno, "Ambiguities in measuring the physical parameters for twisted-nematic liquid crystal spatial light modulators," Opt. Eng. **38**, 705–709 (1999).
8. J. A. Davis, I. Moreno, and P. Tsai, "Polarization eigenstates for twisted-nematic liquid-crystal displays," Appl. Opt. **37**, 937–945 (1998).
9. I. Moreno, J. A. Davis, K. G. D'Nelly, and D. B. Allison, "Transmission and phase measurement for polarization eigenvectors in twisted-nematic liquid crystal spatial light modulators," Opt. Eng. **37**, 3048–3052 (1998).
10. A. Márquez, C. Iemmi, I. Moreno, J. A. Davis, J. Campos, and M. J. Yzuel, "Quantitative prediction of the modulation behavior of twisted nematic liquid crystal displays based on a simple physical model," Opt. Eng. **40**, 2558–2564 (2001).
11. J. Nicolás, J. Campos, and M. J. Yzuel, "Phase and amplitude modulation of elliptic polarization states by nonabsorbing anisotropic elements: application to liquid-crystal devices," J. Opt. Soc. Am. A **19**, 1013–1020 (2002).
12. V. Durán, J. Lancis, E. Tajahuerce, and Z. Jaroszewicz, "Equivalent retarder-rotator approach to on-state twisted nematic liquid crystal displays," J. Appl. Phys. **99**, 113101 (2006).
13. V. Durán, J. Lancis, E. Tajahuerce, and M. Fernández-Alonso, "Phase-only modulation with a twisted nematic liquid crystal display by means of equi-azimuth polarization states," Opt. Express **14**, 5607–5616 (2006).
14. H. Kim and B. Lee, "Optimal nonmonotonic convergence of iterative Fourier-transform algorithm," Opt. Lett. **30**, 296–298 (2005).
15. J. Hahn, H. Kim, K. Choi, and B. Lee, "Real-time digital holographic beam-shaping system with a genetic feedback tuning loop," Appl. Opt. **45**, 915–924 (2006).
16. M. C. Gardner, R. E. Kilpatrick, S. E. Day, R. E. Renton, and D. R. Selviah, "Experimental verification of a computer model for optimizing a liquid crystal display for spatial phase modulation," J. Opt. A: Pure Appl. Opt. **1**, 299–303 (1999).
17. A. Márquez, M. Yamauchi, J. A. Davis, and D. J. Franich, "Phase measurements of a twisted nematic liquid crystal spatial light modulator with a common-path interferometer," Opt. Commun. **190**, 129–133 (2001).
18. J. Reményi, P. Várhegyi, L. Domjan, P. Koppa, and E. Lorincz, "Amplitude, phase, and hybrid ternary modulation modes of a twisted-nematic liquid-crystal display at ~400 nm," Appl. Opt. **42**, 3428–3434 (2003).
19. H. Kim and B. Lee, "Optimal design of diffractive optical elements with functional relationship between phase and amplitude modulations using nonlinear optimization methods," Proc. SPIE **5876**, 587611 (2005).